





Article

A Model for the Proliferation–Quiescence Transition in Human Cells

Kudzanayi Z. Mapfumo ^{1,†} , Jane C. Pagan'a ^{2,†}, Victor Ogesa Juma ^{3,†} , Nikos I. Kavallaris ^{4,†} 
and Anotida Madzvamuse ^{5,6,7,*} 

- ¹ Department of Mathematics and Computational Sciences, University of Zimbabwe, Harare P.O. Box MP167, Zimbabwe; kudzanayi.mapfumo@students.uz.ac.zw
² Department of Statistics and Mathematics, Bindura University of Science Education, Bindura P.O. Box 1020, Zimbabwe; jpaganá@buse.ac.zw
³ Mechanical Engineering Department, University of Zaragoza, Edificio Betancourt, Campus Rio Ebro, E-50018 Zaragoza, Spain; vjuma@unizar.es
⁴ Department of Mathematics and Computer Science, Faculty of Health, Science and Technology, Karlstad University, 651 88 Karlstad, Sweden; nikos.kavallaris@kau.se
⁵ Department of Mathematics, University of Sussex, Pevensey III, Brighton BN1 9QH, UK
⁶ Department of Mathematics, University of Johannesburg, Johannesburg 2006, South Africa
⁷ Department of Mathematics, University of British Columbia, 1984 Mathematics Road, Vancouver, BC V6T 1Z2, Canada
* Correspondence: a.madzvamuse@sussex.ac.uk
† These authors contributed equally to this work.
‡ Conceived the research study.

Abstract: The process of revitalising quiescent cells in order for them to proliferate plays a pivotal role in the repair of worn-out tissues as well as for tissue homeostasis. This process is also crucial in the growth, development and well-being of higher multi-cellular organisms such as mammals. Deregulation of proliferation–quiescence transition is related to many diseases, such as cancer. Recent studies have revealed that this proliferation–quiescence process is regulated tightly by the *Rb – E2F* bistable switch mechanism. Based on experimental observations, in this study, we formulate a mathematical model to examine the effect of the growth factor concentration on the proliferation–quiescence transition in human cells. Working with a non-dimensionalised model, we prove the positivity, boundedness and uniqueness of solutions. To understand model solution behaviour close to bifurcation points, we carry out bifurcation analysis, which is further illustrated by the use of numerical bifurcation analysis, sensitivity analysis and numerical simulations. Indeed, bifurcation and numerical analysis of the model predicted a transition between bistable and stable states, which are dependent on the growth factor concentration parameter (*GF*). The derived predictions confirm experimental observations.

Keywords: cell cycle; proliferation; quiescence; system of ODEs; bifurcation analysis; numerical bifurcation analysis; sensitivity analysis

MSC: 34C23; 65L05



Citation: Mapfumo, K.Z.; Pagan'a, J.C.; Juma, V.O.; Kavallaris, N.I.; Madzvamuse, A. A Model for the Proliferation–Quiescence Transition in Human Cells. *Mathematics* **2022**, *10*, 2426. <https://doi.org/10.3390/math10142426>

Academic Editor: Giancarlo Consolo

Received: 23 May 2022

Accepted: 8 July 2022

Published: 12 July 2022

Publisher's Note: MDPI stays neutral with regard to jurisdictional claims in published maps and institutional affiliations.



Copyright: © 2022 by the authors. Licensee MDPI, Basel, Switzerland. This article is an open access article distributed under the terms and conditions of the Creative Commons Attribution (CC BY) license (<https://creativecommons.org/licenses/by/4.0/>).

1. Introduction

The human body consists of approximately 10^{13} – 10^{14} cells. A large proportion of these cells are quiescent, a biochemically distinct state of growth arrest from which cells can re-enter the cell cycle [1]. The proportion of quiescent cells consists of cells that can no longer be re-activated to re-enter the cell cycle, and cells that can be re-activated to re-enter the cell cycle in response to growth factor signals under normal physiological conditions [2]. The cell cycle comprises four phases, namely: G_1 (first gap phase), S (synthesis phase), G_2 (second gap phase) and M (mitosis), where gap phases refer to the time interval between the synthesis phase and mitosis [3,4]. Here, mitosis refers to the process by which a single cell

divides into two identical daughter cells. The commitment of a cell to cell division is driven by growth factor signals. The availability of sufficient growth factors just beyond a certain point between G_1 and S , known as the restriction point, leads to the progression of the cell cycle process, otherwise the cell enters a reversible state of growth arrest (G_0) [5–12].

Mammalian cellular homeostasis (the state of steady internal, physical, and chemical conditions maintained by cells) depends on the ability of cells to reversibly switch between quiescence and proliferation [13]. This mechanism is crucial for tissue repair and regeneration and is fundamental to the growth, development and well-being of mammals. The decision by cells to exit or enter quiescence is dysregulated in cancer and degenerative diseases [14–16]. Therefore, understanding the molecular mechanisms that control the reversible transition between quiescence and proliferation is crucial and remains a challenging problem in biological and medical sciences. In the 1970s and 1980s, three classes of models were proposed to describe the transition between cellular quiescence and proliferation [17]. These include: the “transition probability” models [18–21], the “growth controlled” models [22,23] and the hybrid models [24,25]. Hybrid models were developed by integrating transition probability- and growth-controlled models [24,25]. Though these models are coherent with diverse experimental data, they lack depth, since they are descriptive. Modelling proliferation–quiescence transition has shifted from this approach since the discovery, in the contexts of molecular and cell biology, of certain genes that regulate proliferation–quiescence transition [17]. Continuum mathematical models describing the temporal dynamics to provide insights into proliferation–quiescence transition within the cell cycle using gene regulatory networks have been proposed in the last two decades [26–35]. Limit cycles [28,30,32], cell-mass-regulated bi-stable systems [25,34,36], bi-stable and excitable systems [33,37] and transient processes [26,29,38] are examples of the cell-cycle dynamics deduced through cell-cycle modelling. It has been demonstrated experimentally that proliferation–quiescence transition is controlled by the $Rb - E2F$ signalling network, which acts as a bi-stable switch [17]. Here, Rb and $E2F$ represent the Retinoblastoma and Transcription factors respectively. Previously, models for the regulation of the $Rb - E2F$ have been put forward and simulated [29,32,38], with more details provided in the model proposed by Aguda and Tang [38]. At the heart of the regulation of the $Rb - E2F$ signalling network are: cyclin D ($CycD$), cyclin E ($CycE$), cyclin A ($CycA$), cyclin-dependent kinases ($CDKs$), family of transcription factors $E2F$, Myc and the retinoblastoma (Rb) family of proteins [39,40]. The retinoblastoma (Rb) protein family is responsible for regulating proliferation in most cells. The $E2F$ family of transcription factors is responsible for the regulation of genes involved in DNA replication and cell cycle progression [41,42]. Interactions among these regulators have been outlined and verified experimentally [17]. However, due to the complex nature of the $Rb - E2F$ network, which consists of criss-crossing linkages, a clear description of the proliferation–quiescence transition is elusive. In this study, we simplify the $Rb - E2F$ signalling network that has been theoretically and experimentally verified in [43–46], and formulate an activator-inhibitor model system following the same philosophy as that proposed by Tyson et al. in [25], to analyse the proliferation–quiescence transition. To investigate the dynamics of the $Rb - E2F$ signalling network describing proliferation–quiescence transition, we have taken the approach of combining redundant and overlapping cellular activities and collapsing linear cascades, as presented by Yao et al. [42], to simplify the model to three nodes connected by activation and inhibition links, as experimentally verified in [45]. Although the terms activation and inhibition are generally used in the literature, in this study we will also refer to these molecular processes as the production/synthesis and degradation/removal of abundant species, respectively. In addition, we consider the conservation of the total concentration of the Rb family of proteins and show through bifurcation and numerical analysis that the resulting system generates a set of three dynamical behaviours shown in experiments [1,2,17]; namely, stability, bistability and stability when the growth factor concentration (GF) is varied. Bifurcation and numerical analysis also show that quies-

cence is achieved under low growth factor stimulation and proliferation requires strong growth-factor stimulation.

This paper is organised as follows: in Section 2, we utilise the current understanding of activator-inhibitor systems and apply biologically reasonable assumptions to motivate a system of non-linear ordinary differential equations (ODEs) and describe the pertinent interactions. In the same section, we non-dimensionalise the system, outline positivity, boundedness and prove the existence and uniqueness of solutions. This section ends with a further study of the non-linear ODE system to gain insights into its stability behaviour. In Section 3, we conduct a bifurcation analysis of the model to analyse the effect of varying the growth factor concentration on the steady states of the system. We also conduct numerical simulations to illustrate, computationally, the theoretical results. The last part of Section 3 presents sensitivity analysis for parameters of the system. We discuss the interpretations and implications of our results in Section 4. Finally, in Section 5, we discuss the limitations of our study and present possible future research problems.

2. Materials and Methods

2.1. Proliferation–Quiescence Dynamics Model

Our mathematical model is formulated based on first principles by first simplifying the $Rb - E2F$ model studied by Yao et al. [17], collapsing all the several reaction networks into three main nodes denoted by: R , M and E and thus reducing the reaction links from 10 to 8, as shown in Figure 1. The R node consists of the Rb family of proteins ($Rbp107$ and $Rbp108$), the E node consists of the family of transcription factors $E2F$, Cyclin E and Cyclin A , and the M node consists of cyclin D and Myc . Experimentally, it is observed that R proteins are conserved throughout, while those of M and E are not [40]. Due to lack of experimental justifications for some reactions, and following other published works [12,40], in formulating our model we will employ Michaelis–Menten kinetics, mass action as well as the Hill function [47]. Michaelis–Menten kinetics describe the rate of enzymatic reactions by relating reaction rates to the concentration of a substrate, while the law of mass action states that the rate of a chemical reaction is directly proportional to the product of the activities or concentrations of the reactants [48,49].

Yao et al. [17] represented the three respective nodes by symbols: RP , EE and MD . These nodes are connected by 10 regulatory linkages. In their model, they assumed activation of the three species RP , EE and MD by Hill functions of the form: $\frac{A^n}{K^n + [A]^n}$, where A represents any of the three species RP , MD or EE , K is a Michaelis–Menten constant and $1 \leq n \leq 10$. In addition, they assumed that the inhibition of RP , EE and MD was through mass action kinetics. Of interest was their exclusion of the constitutive synthesis of EE together with its self-activation and the conservation of mass of the RP family of proteins, which we will consider in our model. Moreover, they considered self-inhibition of EE and inhibition of EE by MD , which we removed in our model. The simplified network self-reorganises to form an activator-inhibitor network, as shown in Figure 1.

In our model formulation, we ignore the spatial localisation of the proteins; such an extension forms part of our current studies and is beyond the scope of this work. We note, however, that such an approach leads naturally to partial differential equations. The resulting model, when spatial effects are neglected, is given in terms of a system of non-linear ordinary differential equations (ODEs) describing the rate of change in the concentrations of $M(t)$, $R(t)$ and $E(t)$. The main novelty of the model is the use of the Hill function with $n = 2$ to describe kinetics with saturation. The model is formulated based on the following assumptions:

- 1 The production of $M(t)$ is through mass action by extra-cellular growth signals GF and by $E(t)$, which is modelled using Michaelis–Menten kinetics, whereas its decay is modelled by mass action. Yao et al. [2] considered Michaelis–Menten kinetics for the production of $M(t)$ through extra-cellular growth signals.
- 2 The activation of $R(t)$ is enhanced by $E(t)$ and its inhibition is intensified by $M(t)$ and $E(t)$, which are both modelled using mass action. It is pertinent to note that, in this

study, we assume conservation of mass for the *Rb* family of proteins, which was not considered in [2]. In addition, we assume self-activation and inhibition of $R(t)$ using the Hill function with $n = 2$. On the contrary, Yao et. al. [2] modelled the production and depletion of $R(t)$ using Michaelis–Menten kinetics and mass action, respectively, and self-activation and de-activation were not considered.

- 3 $E(t)$ is synthesised, cf. [40], with the use of Michaelis–Menten kinetics and its synthesis is enhanced by $M(t)$ with the use of a Hill function with $n = 2$, while its decay is enhanced by $R(t)$ with the use of mass action. On the contrary, the authors in [2] did not consider constitutive synthesis of $E(t)$, which has been observed experimentally as indicated in [40].

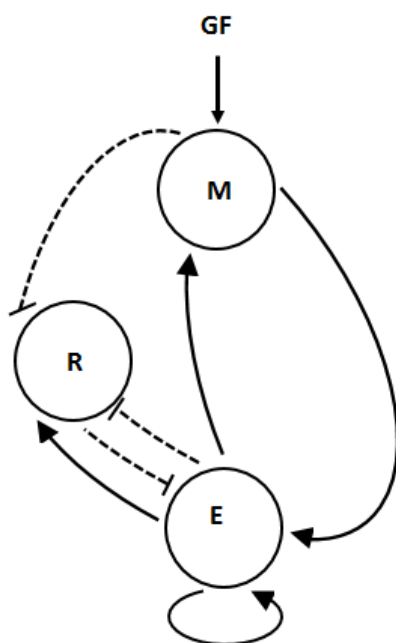


Figure 1. An activator-inhibitor network for the *Rb* – *E2F* signalling network [42]. The solid arrows represent activation mechanism while the broken lines represent inhibition. Here, the growth factors *GF* activate *M* (cyclin *D* and *Myc*) and, in turn *M* activates *E* (cyclin *A*, cyclin *E* and *E2F* transcription factors) while *E* activates *M*, forming a positive feedback loop. *R* (*Rb* family of proteins) inhibits *E*, while *E* activates and inhibits *R* and *M* inhibits *R*.

The main novelty of our proposed model is that we consider mass conservation of the *Rb* family of proteins represented by $R(t)$ existing in both hypo-phosphorylated form denoted by $R_u(t)$ and hyper-phosphorylated form denoted by $R_p(t)$; whereas in [42] it was assumed that the concentration of the *Rb* family of proteins was abundant and hence there was no mass conservation. This assumption makes our model more realistic, as the transition from cellular quiescence to proliferation is dependent on the cycling between the hyper-phosphorylated and hypo-phosphorylated forms of *Rb* family of proteins mediated by cyclin-dependent kinases. Hyperphosphorylation of *Rb* enhances proliferation, whereas hypo-phosphorylated *Rb* enhances quiescence [50]. In addition, some reaction pathways were not considered in [2], including constitutive synthesis of *E* and the simple mass action for the activation of $R(t)$. Therefore, employing mass conservation, the total concentration of $R(t)$ is such that:

$$R_u(t) + R_p(t) = R_T = \text{Constant}.$$

The state variable $R(t)$ denotes the concentration of $R_p(t)$ at time t in the model. $R_u(t)$ corresponds to the inactive term $R_T - R$ used in Equation (1c). Therefore, the time evolution of $M(t)$, $E(t)$ and $R(t)$ are, respectively, described by the following system of non-linear ordinary differential equations (ODEs):

$$\frac{dM}{dt} = \underbrace{\alpha_1 GF}_{\text{production of } M \text{ by } GF} + \underbrace{\frac{\beta_1 ME}{k_1 + E}}_{\text{production of } M \text{ by } E} - \underbrace{\delta M}_{\text{decay of } M}, \quad (1a)$$

$$\frac{dE}{dt} = \underbrace{\alpha_6}_{\text{E baseline value}} + \underbrace{\frac{\alpha_4 E}{\alpha_8 + E}}_{\text{E constitutive-synthesis}} + \underbrace{\frac{\beta_4 EM^2}{k_{r_3}^2 + M^2}}_{\text{Production of } E \text{ by } M} - \underbrace{\alpha_5 RE}_{\text{removal of } E \text{ by } R}, \quad (1b)$$

$$\begin{aligned} \frac{dR}{dt} = & \underbrace{\frac{\beta_2(R_T - R)E}{k_{r_1}^2 + (R_T - R)^2}}_{\text{Activation of } R \text{ by } E} + \underbrace{\frac{\beta_3(R_T - R)^2}{k_{r_1}^2 + (R_T - R)^2}}_{\text{R baseline activation}} - \underbrace{\alpha_2 RM}_{\text{Inhibition of } R \text{ by } M} - \underbrace{\alpha_3 RE}_{\text{inhibition of } R \text{ by } E} \\ & - \underbrace{\frac{\beta_5 R^2}{k_{r_2}^2 + R^2}}_{\text{R baseline inhibition}}. \end{aligned} \quad (1c)$$

The system is closed with non-negative initial conditions $M(0) = M_0$, $E(0) = E_0$, and $R(0) = R_0$, $0 \leq M(t)$, $E(t)$ and $0 \leq R(t) \leq R_T$. In our model, we consider M and E families of proteins to exist in abundance; hence, there is no conservation of mass, unlike the Rb family of proteins, which is conserved as outlined in the model formulation. This implies, that for some appropriate model parameter values, M and E might be unbounded. Model parameters are chosen based on a previous modelling study on the $Rb - E2F$ pathway [17]. All model parameters are strictly positive and their values, units and physical meaning are described in Table 1.

Table 1. Parameters used for simulations and bifurcation analysis. Parameter values are taken from [17,42] and some of them adjusted to illustrate the qualitative dynamics. Here, U represents the unit of concentration and s the unit of time t .

Parameter	Description	Value	Units	Reference
α_1	Growth factors activation rate	1	s^{-1}	[17]
GF	Growth factors concentration	varies	U	[42]
δ	Inhibition rate of M	1.001	s^{-1}	[17]
k_1	Michaelis–Menten constant	1	U	[42]
β_1	Activation rate of M	1	s^{-1}	[42]
β_2	Activation of R protein family	1	$U^{-1}s^{-1}$	[42]
α_3	Inhibition rate of R by E	1	$U^{-1}s^{-1}$	Estimate
α_2	Inhibition rate of R by M	1	$U^{-1}s^{-1}$	Estimate
β_3	R baseline inhibition rate	1	Us^{-1}	Estimate
R_T	Total concentration of R	5	U	[40]
α_4	E self activation rate	0.02	Us^{-1}	[17]
β_4	Activation rate E by M	0.02	s^{-1}	[17]
β_5	R baseline inhibition rate	1	Us^{-1}	Estimate
α_6	E constitutive activation rate	0.001	s^{-1}	[40]
α_8	Michaelis–Menten constant	0.92	U	[42]
α_5	Inhibition rate of E by R	0.01	$U^{-1}s^{-1}$	[42]
k_{r_1}	Michaelis–Menten constant	0.05	U	[42]
k_{r_2}	Michelis–Menten constant	1	U	[42]
k_{r_3}	Michaelis–Menten constant	1	U	[42]

2.2. Mathematical Analysis of the Model

In this section, we non-dimensionalise system (1) so that it is unit free for purposes of mathematical analysis, including proving positivity, boundedness, existence and uniqueness of solutions as well as performing the sensitivity analysis. However, numerical bifurcation and numerical simulations were performed on the dimensional model. This is meant to preserve the original concentration of species GF, which appears in Equation (1a).

2.3. Non-Dimensionalisation

There are nineteen parameters in system (1). We can reduce the number of parameters to sixteen by defining new coordinates $M = Xx^*$, $E = Yy^*$, $R = Zz^*$ and $t = T\tau$, where X, Y, Z and t are constant (dimension carrying) scales, to be chosen and $x^*; y^*; z^*; \tau$ are the numerical (dimensionless) variables. Substituting these into (1) and letting $a_1 = \frac{\alpha_1 GF}{\alpha_4}$, $a_2 = \frac{\beta_1 \alpha_8}{\alpha_4}$, $a_3 = \frac{k_1}{\alpha_8}$, $a_4 = \frac{\delta \alpha_8}{\alpha_4}$, $a_5 = \frac{\beta_2 \alpha_8^2}{\alpha_4}$, $a_6 = \frac{R_T}{\alpha_8}$, $a_7 = \frac{\beta_3}{\alpha_4}$, $a_8 = \frac{k_{r1}^2}{\alpha_8^2}$, $a_9 = \frac{\alpha_2 \alpha_8^2}{\alpha_4}$, $a_{10} = \frac{\alpha_3 \alpha_8^2}{\alpha_4}$, $a_{11} = \frac{\beta_5}{\alpha_4}$, $a_{12} = \frac{k_{r2}^2}{\alpha_8^2}$, $a_{13} = \frac{\beta_4 \alpha_8}{\alpha_4}$, $a_{14} = \frac{k_{r3}^2}{\alpha_8^2}$, $a_{15} = \frac{\alpha_6 \alpha_8}{\alpha_4}$ and $a_{16} = \frac{\alpha_5 \alpha_8^2}{\alpha_4}$, and, dropping $*$ so that $x^* = x$, $y^* = y$ and $z^* = z$, we obtain the non-dimensional system:

$$\frac{dx}{dt} = a_1 + \frac{a_2 xy}{a_3 + y} - a_4 x, \quad (2a)$$

$$\frac{dy}{dt} = a_{16} + \frac{y}{1+y} + \frac{a_{13} x^2 y}{a_{14} + x^2} - a_{15} y z, \quad (2b)$$

$$\frac{dz}{dt} = a_5(a_6 - z)y + \frac{a_7(a_6 - z)^2}{a_8 + (a_6 - z)^2} - a_9 x z - a_{10} y z - \frac{a_{11} z^2}{a_{12} + z^2}, \quad (2c)$$

with positive initial conditions $x(0) = x_0$, $y(0) = y_0$ and $z(0) = z_0$ and positive constant parameters a_1, \dots, a_{16} .

2.4. Positivity, Boundedness and Existence and Uniqueness of Solutions

We first show that system (2), associated with initial conditions, has a unique local solution.

Lemma 1 (Local existence and uniqueness). *System (2), associated with the initial condition $(x(0), y(0), \text{and } z(0))$, has a unique local solution in the interval $(0, T)$ for some $T > 0$.*

Proof. System (2) can be written in matrix form, as follows:

$$\frac{d\vec{x}}{dt} = \begin{bmatrix} \frac{dx}{dt} \\ \frac{dy}{dt} \\ \frac{dz}{dt} \end{bmatrix} = \vec{f}(\vec{x}) = \begin{bmatrix} f_1(x, y, z) \\ f_2(x, y, z) \\ f_3(x, y, z) \end{bmatrix}, \quad (3)$$

for $\vec{x} = \vec{x}(t) = (x(t), y(t), z(t))^T$ and

$$\begin{aligned} f_1(x, y, z) &:= a_1 + \frac{a_2 xy}{a_3 + y} - a_4 x, \\ f_2(x, y, z) &:= a_{16} + \frac{y}{1+y} + \frac{a_{13} x^2 y}{a_{14} + x^2} - a_{15} y z, \\ f_3(x, y, z) &:= a_5(a_6 - z)y + \frac{a_7(a_6 - z)^2}{a_8 + (a_6 - z)^2} - a_9 x z - a_{10} y z - \frac{a_{11} z^2}{a_{12} + z^2}. \end{aligned}$$

It follows that \vec{f} is Lipschitz continuous, i.e., there exists a constant $L \geq 0$ such that $\|\vec{f}(\vec{x}_1) - \vec{f}(\vec{x}_2)\| \leq L\|\vec{x}_1 - \vec{x}_2\|$, for all $\vec{x}_1, \vec{x}_2 \in D$, for any bounded region D in \mathbb{R}_+^3 . Then, local existence and uniqueness of solutions is established by the classic theory, cf. [51]. \square

Next, the positivity of solutions of (2) is established; hence, the feasibility of solutions for the study of the underlying biological problem is guaranteed.

Lemma 2 (Positivity). *If the initial condition in system (2) satisfies $x(0) > 0, y(0) > 0, z(0) > 0$, then the solution $(x(t), y(t), z(t))$ of (2) will remain in \mathbb{R}_+^3 for all $t \in [0, T]$, where $T > 0$ stands for the maximum existence time guaranteed by Lemma 1.*

Proof. We must prove that $(x(t), y(t), z(t))$ will remain in \mathbb{R}_+^3 for any $t \in (0, T)$, where $T > 0$ is the maximum existence time. Since $x(0) > 0, y(0) > 0, z(0) > 0$ then, by a continuity argument, there exists $t_1 > 0$ such that $(x(t), y(t), z(t)) \in \mathbb{R}_+^3$ for all $t \in [0, t_1]$. Thus, recalling that all parameters used in system (2) are positive, we derive the following inequalities in the interval $(0, t_1)$

$$\frac{dx}{dt} = a_1 + \frac{a_2xy}{a_3 + y} - a_4x \geq -a_4x, \quad (4a)$$

$$\frac{dy}{dt} = a_{16} + \frac{y}{1 + y} + \frac{a_{13}x^2y}{a_{14} + x^2} - a_{15}yz \geq -a_{15}yz, \quad (4b)$$

$$\frac{dz}{dt} = a_5(a_6 - z)y + \frac{a_7(a_6 - z)^2}{a_8 + (a_6 - z)^2} - a_9xz - a_{10}yz - \frac{a_{11}z^2}{a_{12} + z^2} \geq -a_5z - a_9xz - a_{10}yz. \quad (4c)$$

Now, integrating the above differential equation inequalities in the interval $[t_1, T)$, we obtain

$$\begin{aligned} x(t) &\geq A_0 e^{-a_4(t-t_1)} > 0, \\ y(t) &\geq C_0 e^{-a_{15} \int_{t_1}^t z(t) dt} > 0, \\ z(t) &\geq B_0 e^{-a_9 \int_{t_1}^t x(t) dt - (a_5 + a_{10}) \int_{t_1}^t y(t) dt} > 0, \end{aligned}$$

for some positive constants A_0, B_0, C_0 . Thus, for all $t \in [0, t_1]$, $x(t), y(t)$, and $z(t)$ will remain in \mathbb{R}_+^3 . Repeating this argument, we can prove that $(x(t), y(t), z(t)) \in \mathbb{R}_+^3$ for any $t \in (0, T)$, and this completes the proof. \square

Lemma 3 (Boundedness). *There exists $x_v, y_v, z_v > 0$ such that $\limsup_{t \rightarrow T} x(t) \leq x_v$, $\limsup_{t \rightarrow T} y(t) \leq y_v$ and $\limsup_{t \rightarrow T} z(t) \leq z_v$ provided that $\min(\theta, \phi) > 0$ where $\theta := a_4 - a_2$ and $\phi := a_{15}z_v - a_{13}$. Here, T is the maximum existence time for system (2) given by Lemma 1.*

Proof. Since all involved constants $a_i, i = 1, \dots, 16$ are positive, thanks to Lemma 2 we can deduce that

$$\lim_{z \rightarrow a_6} \frac{dz}{dt} = -a_6a_9x - a_6a_{10}y - \frac{a_{11}a_6^2}{a_{12} + a_6^2} \leq 0,$$

which implies that there exists $z_v > 0$ such that $\limsup_{t \rightarrow T} z(t) \leq z_v$; hence, $z(t)$ is bounded in $[0, T]$. By making the substitution $z = z_v$ we also obtain that

$$\begin{aligned} \frac{dx}{dt} + \frac{dy}{dt} &= a_1 + \frac{a_2xy}{a_3 + y} - a_4x + a_{16} + \frac{y}{y + 1} + \frac{a_{13}x^2y}{a_{14} + x^2} - a_{15}yz_v \\ &\leq a_1 + a_2x - a_4x + a_{16} + 1 + a_{13}y - a_{15}yz_v, \\ &\leq a_1 + a_{16} + 1 - x(a_4 - a_2) - y(a_{15}z_v - a_{13}). \end{aligned}$$

Setting $\theta := a_4 - a_2$ and $\phi := a_{15}z_v - a_{13}$, provided that $\min(\theta, \phi) > 0$, then it follows that

$$\frac{d(x + y)}{dt} \leq \lambda - \theta x - \phi y \leq \lambda - \min(\theta, \phi)(x + y),$$

where $\lambda := a_1 + a_{16} + 1$. Solving this differential inequality using the method of integrating factor, we obtain:

$$(x + y)(t) \leq \frac{\lambda}{\min(\theta, \phi)} + c_0 e^{-\min(\theta, \phi)t} \leq \frac{\lambda}{\min(\theta, \phi)} + c_0,$$

and thus

$$\limsup_{t \rightarrow T} (x + y)(t) \leq \frac{\lambda}{\min(\theta, \phi)} + c_0.$$

Now, choosing

$$x_v = y_v = \frac{\lambda}{\min(\theta, \phi)} + c_0;$$

entails that $(x + y)(t)$ is bounded from above and, therefore, $x(t)$, and $y(t)$ are also bounded from above by $x_v = y_v$ for all $t \in [0, T]$. \square

Theorem 1. Under the assumption of Lemma 3 and provided that $x(0), y(0), z(0) > 0$, then system (2) has a global-in-time positive solution; that is, $(x(t), y(t), z(t))$ will exist in \mathbb{R}_+^3 and is bounded for any $t > 0$.

Proof. The existence of a local positive solution for system (2) is an immediate consequence of Lemmas 1 and 2. Thanks to Lemma 2, such a solution is also bounded in $(0, T)$ and, thus, the classical theory, cf. [51] (Corollary 2.3.2), guarantees its existence as a (global) positive solution for all $t > 0$. \square

Next, we demonstrate the existence of at least three uniform states for the model system (1).

2.5. Steady States

The uniform steady state (M^*, E^*, R^*) of System (1) is a solution to the following system of nonlinear algebraic equations

$$\alpha_1 GF + \frac{\beta_1 ME}{k_1 + E} - \delta M = 0, \quad (5)$$

$$\alpha_6 + \frac{\alpha_4 E}{\alpha_8 + E} + \frac{\beta_4 EM^2}{k_{r_3}^2 + M^2} - \alpha_5 RE = 0, \quad (6)$$

$$\beta_2 (R_T - R)E + \frac{\beta_3 (R_T - R)^2}{k_{r_1}^2 + (R_T - R)^2} - \alpha_2 RM - \alpha_3 RE - \frac{\beta_5 R^2}{k_{r_2}^2 + R^2} = 0. \quad (7)$$

Analytically, solving this set of equations gives a cubic polynomial which, by the Fundamental theorem of algebra [52], yields at most three steady states. The illustration of this is shown by plotting numerical bifurcation analysis results shown in Figure 2. Therefore, for some parameter values, system (1) admits up to three steady states, if they exist. We remark that finding exact analytical solutions of the uniform steady states was not possible due to the intractability of the system. Instead, we used bifurcation analysis to unravel the existence of such states.

2.6. Linear Stability Analysis

The following analysis establishes the stability of the positive steady states for ODE system (1). To investigate the stability of (1), we linearize it around the steady state (M^*, E^*, R^*) to obtain:

$$\begin{bmatrix} \frac{d(M - M^*)}{dt} \\ \frac{d(E - E^*)}{dt} \\ \frac{d(R - R^*)}{dt} \end{bmatrix} = \mathcal{J} \begin{bmatrix} M - M^* \\ E - E^* \\ R - R^* \end{bmatrix}, \quad (8)$$

where

$$\mathcal{J} = \begin{bmatrix} \frac{\partial g_1}{\partial M} & \frac{\partial g_1}{\partial E} & \frac{\partial g_1}{\partial R} \\ \frac{\partial g_2}{\partial M} & \frac{\partial g_2}{\partial E} & \frac{\partial g_2}{\partial R} \\ \frac{\partial g_3}{\partial M} & \frac{\partial g_3}{\partial E} & \frac{\partial g_3}{\partial R} \end{bmatrix}_{(M^*, E^*, R^*)}. \quad (9)$$

with

$$\begin{aligned} g_1(M, E, R) &= \alpha_1 GF + \frac{\beta_1 ME}{k_1 + E} - \delta M, \\ g_2(M, E, R) &= \alpha_6 + \frac{\alpha_4 E}{\alpha_8 + E} + \frac{\beta_4 EM^2}{k_3^2 + M^2} - \alpha_5 RE, \\ g_3(M, E, R) &= \beta_2(R_T - R)E + \frac{\beta_3(R_T - R)^2}{k_{r1}^2 + (R_T - R)^2} - \alpha_2 RM - \alpha_3 RE - \frac{\beta_5 R^2}{k_{r2}^2 + R^2}, \end{aligned}$$

and, thus,

$$\begin{aligned} \left. \frac{\partial g_1}{\partial M} \right|_{(M^*, E^*, R^*)} &= -\delta + \frac{\beta_1 E^*}{k_1 + E^*} := \omega_1, \\ \left. \frac{\partial g_1}{\partial E} \right|_{(M^*, E^*, R^*)} &= \frac{k_1 \beta_1 M^*}{(k_1 + E^*)^2} := \omega_2 > 0, \\ \left. \frac{\partial g_1}{\partial R} \right|_{(M^*, E^*, R^*)} &= 0, \\ \left. \frac{\partial g_2}{\partial M} \right|_{(M^*, E^*, R^*)} &= \frac{2M^* \beta_4 E^* k_3^2}{(k_3^2 + M^{*2})^2} := \gamma_1 > 0, \\ \left. \frac{\partial g_2}{\partial E} \right|_{(M^*, E^*, R^*)} &= \frac{\alpha_4 \alpha_8}{(\alpha_8 + E^*)^2} + \frac{\beta_4 M^{*2}}{k_3^2 + M^{*2}} - \alpha_5 R^* := \gamma_2, \\ \left. \frac{\partial g_2}{\partial R} \right|_{(M^*, E^*, R^*)} &= -\alpha_5 E^* := \gamma_3 < 0, \\ \left. \frac{\partial g_3}{\partial M} \right|_{(M^*, E^*, R^*)} &= -\alpha_2 R^* := \theta_1 < 0, \\ \left. \frac{\partial g_3}{\partial E} \right|_{(M^*, E^*, R^*)} &= \beta_2(R_T - R^*) - \alpha_2 R^* := \theta_2, \\ \left. \frac{\partial g_3}{\partial R} \right|_{(M^*, E^*, R^*)} &= -\beta_2 E^* - \frac{2(R_T - R^*)^2 \beta_3 k_{r1}^2}{[k_{r1}^2 + (R_T - R^*)^2]^2} := \theta_3 < 0, \end{aligned}$$

recalling that, due to Theorem 1. it also holds that $(M^*, E^*, R^*) \in \mathbb{R}_+^3$.

Theorem 2. Assume that (M^*, E^*, R^*) is the steady-state solution of ODE system (1). Given that

- (A). $\omega_1, \gamma_2 < 0$ and $\theta_2 > 0$,
 (B). $\omega_1\theta_2 < \omega_2\theta_1$ and $\omega_2\gamma_1 < \omega_1\gamma_2$,
 (C). $\omega_2\theta_1\gamma_3 + \omega_1\omega_2\gamma_1 > 0$ and $\gamma_2\gamma_3\theta_2 + \omega_2\gamma_1\gamma_2 > 0$, then (M^*, E^*, R^*) is asymptotically stable.

Proof. The Jacobian matrix for the system is given by

$$\mathcal{J} = \begin{pmatrix} \omega_1 & \omega_2 & 0 \\ \gamma_1 & \gamma_2 & \gamma_3 \\ \theta_1 & \theta_2 & \theta_3 \end{pmatrix}. \quad (10)$$

Next, we compute the eigenvalues of \mathcal{J} by solving the equation

$$|\mathcal{J} - \lambda I| = \begin{vmatrix} \omega_1 - \lambda & \omega_2 & 0 \\ \gamma_1 & \gamma_2 - \lambda & \gamma_3 \\ \theta_1 & \theta_2 & \theta_3 - \lambda \end{vmatrix} = 0, \quad (11)$$

where I is the 3×3 identity matrix. The characteristic polynomial of \mathcal{J} is then given by

$$\lambda^3 + p_1\lambda^2 + p_2\lambda + p_3 = 0, \quad (12)$$

with coefficients,

$$\begin{aligned} p_1 &= -(\omega_1 + \gamma_2 + \theta_3), \\ p_2 &= \omega_1\gamma_2 + \omega_1\theta_3 + \gamma_2\theta_3 - \gamma_3\theta_2 - \omega_2\gamma_1, \\ p_3 &= \omega_1\gamma_3\theta_2 - \omega_1\gamma_2\theta_3 + \omega_2\gamma_1\theta_3 - \omega_2\gamma_3\theta_1. \end{aligned}$$

By the Routh–Hurwitz stability criterion, all the roots of (12) have negative real parts if $p_1 > 0$, $p_3 > 0$ and $p_1p_2 - p_3 > 0$. Clearly $p_1 > 0$ by condition (A). In addition,

$$\begin{aligned} p_3 &= \omega_1\gamma_3\theta_2 - \omega_2\gamma_3\theta_1 + \omega_2\gamma_1\theta_3 - \omega_1\gamma_2\theta_3 \\ &= \gamma_3(\omega_1\theta_2 - \omega_2\theta_1) + \theta_3(\omega_2\gamma_1 - \omega_1\gamma_2) \end{aligned}$$

and, thus, by conditions (A) and (B) it follows that $p_3 > 0$.

It remains to show that $p_1p_2 - p_3 > 0$. Now,

$$\begin{aligned} p_1p_2 - p_3 &= -(\omega_1 + \gamma_2 + \theta_3)(\omega_1\gamma_2 + \omega_1\theta_3 + \gamma_2\theta_3 - \gamma_3\theta_2 - \omega_2\gamma_1) \\ &\quad - (\omega_2\gamma_1\theta_3 + \omega_1\gamma_3\theta_2 - \omega_1\gamma_2\theta_3 - \omega_2\theta_1\gamma_3). \end{aligned}$$

After simplifying and grouping, we obtain

$$\begin{aligned} p_1p_2 - p_3 &= -\omega_1^2\gamma_2 - \omega_1^2\theta_3 + \omega_1\omega_2\gamma_1 - \omega_1\gamma_2^2 - \omega_1\gamma_2\theta_3 - \gamma_2^2\theta_3 + \gamma_2\gamma_3\theta_2 \\ &\quad + \omega_2\gamma_1\gamma_2 - \omega_1\gamma_2\theta_3 - \omega_1\theta_3^2 - \gamma_2\theta_3^2 + \gamma_3\theta_2\theta_3 + \omega_2\theta_1\gamma_3 \\ &= -\omega_1^2\gamma_2 - \omega_1^2\theta_3 + \omega_2\theta_1\gamma_3 + \omega_1\omega_2\gamma_1 - \omega_1\gamma_2^2 - \omega_1\gamma_2\theta_3 - \gamma_2^2\theta_3 \\ &\quad + \gamma_2\gamma_3\theta_2 + \omega_2\gamma_1\gamma_2 - \omega_1\gamma_2\theta_3 - \omega_1\theta_3^2 - \gamma_2\theta_3^2 + \gamma_3\theta_2\theta_3. \end{aligned}$$

Due to conditions (A)–(C) and in conjunction with the sign of the parameter $\theta_3 < 0$, then $p_1p_2 - p_3 > 0$. Hence, the system of ODEs (1) becomes asymptotically stable. \square

3. Results

3.1. Bifurcation Analysis

Bifurcation analysis of the system of ODEs (1) was carried out using XPPAUT, a software program freely available from <https://asmedigitalcollection.asme.org/appliedmechanicsreviews/article/56/4/B53/463898/Simulating-Analyzing-and-Animating-Dynamical> (accessed on 22 November 2020) [53]. Parameter values for our model are shown in Table 1,

unless otherwise specified. The parameter values were chosen based on the literature whenever possible and some of them adjusted to illustrate qualitative dynamics [17,42]. As shown in Figure 2a, there exists a unique steady state corresponding to the quiescent state when $GF < 0.3735$ with $M^* < 1.225$. For $0.3735 < GF < 0.4138$, bistable dynamics result from a saddle node bifurcation marked by two black dots labelled as SN (saddle node). As GF increases further out of the bistable regime, M^* jumps into its high steady state, where a cell undergoes proliferation. We also plot k_1 against GF and generate a two parameter bifurcation diagram shown in Figure 2c. In the latter figure, the bistable region is coloured green.

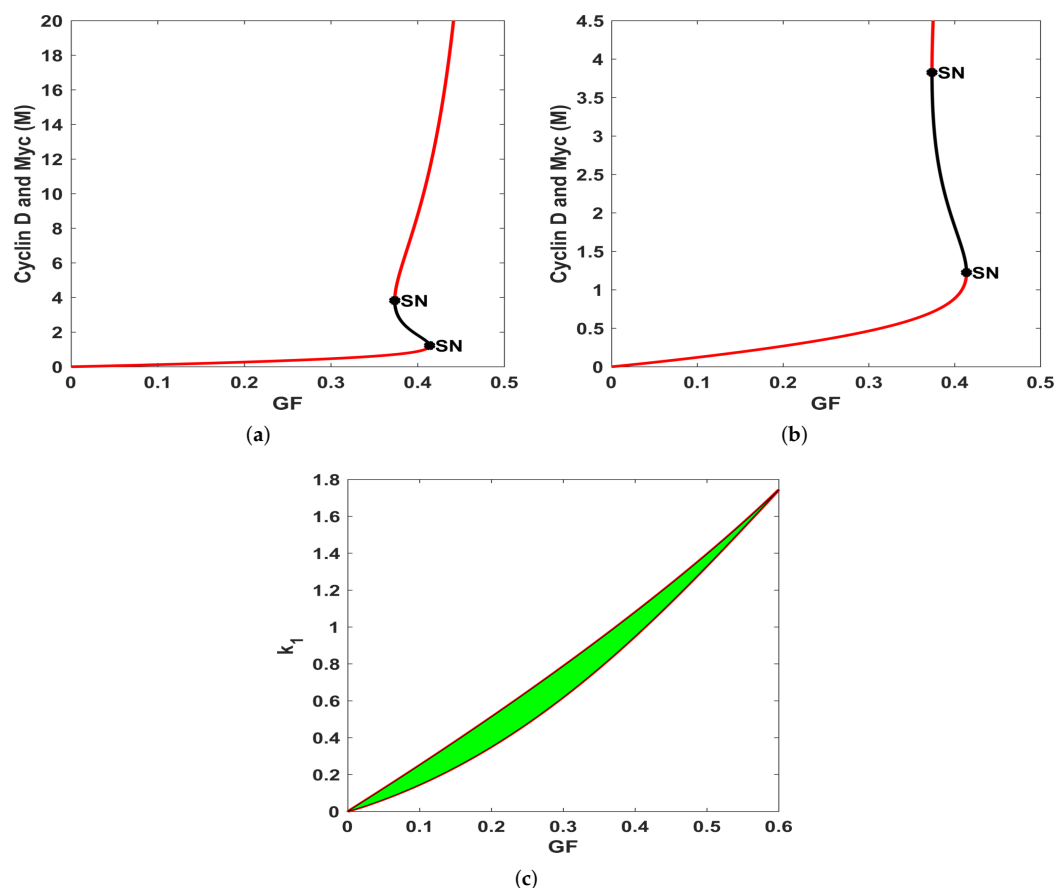


Figure 2. Numerical bifurcation diagrams for the system of ODEs (1), with parameter values listed in Table 1. (a) One parameter bifurcation diagram for M^* , with the growth factor GF concentration value as a bifurcation parameter. The saddle-node (SN) bifurcation points for GF are 0.3735 and 0.4138 and the corresponding M^* are 3.826 and 1.225, respectively. The red line represents the stable steady states whereas the thin black line represent saddle points. The black dots labelled SN are the saddle-node bifurcation points, which span the region characterised by bistable dynamics. (b) A one-parameter bifurcation diagram showing a zoom of (a) around the two saddle-node bifurcation points. (c) Two-parameter bifurcation diagram with k_1 and GF as bifurcation parameters. The green coloured region is characterised by bistable dynamics, whereas the colourless region is characterised by stable dynamics.

3.2. Numerical Simulations

Numerical simulations were carried out using the MATLAB ode45 solver [54]. This is a standard solver for ordinary differential equations (ODEs) that implements a Runge–Kutta method with a variable time-step for efficient computations, (see [55] for details). We simulated the system by selecting values of GF corresponding to different dynamic regimes deduced through the bifurcation analysis in the previous subsection. We solved the system

of ODEs (1) for those three regimes and plot the solution for separate time intervals with a variable growth factor concentration value and for different initial conditions.

First, we show the time evolution for $M(t)$, $R(t)$ and $E(t)$ by solving numerically system (1) with parameters as outlined in Table 1 assuming the growth factor has concentration value $GF = 0.3$ with initial conditions $M_0 = 0.2$, $E_0 = 1.2$ and $R_0 = 3$, which bring the system to the lower stable region, as shown in Figure 3a.

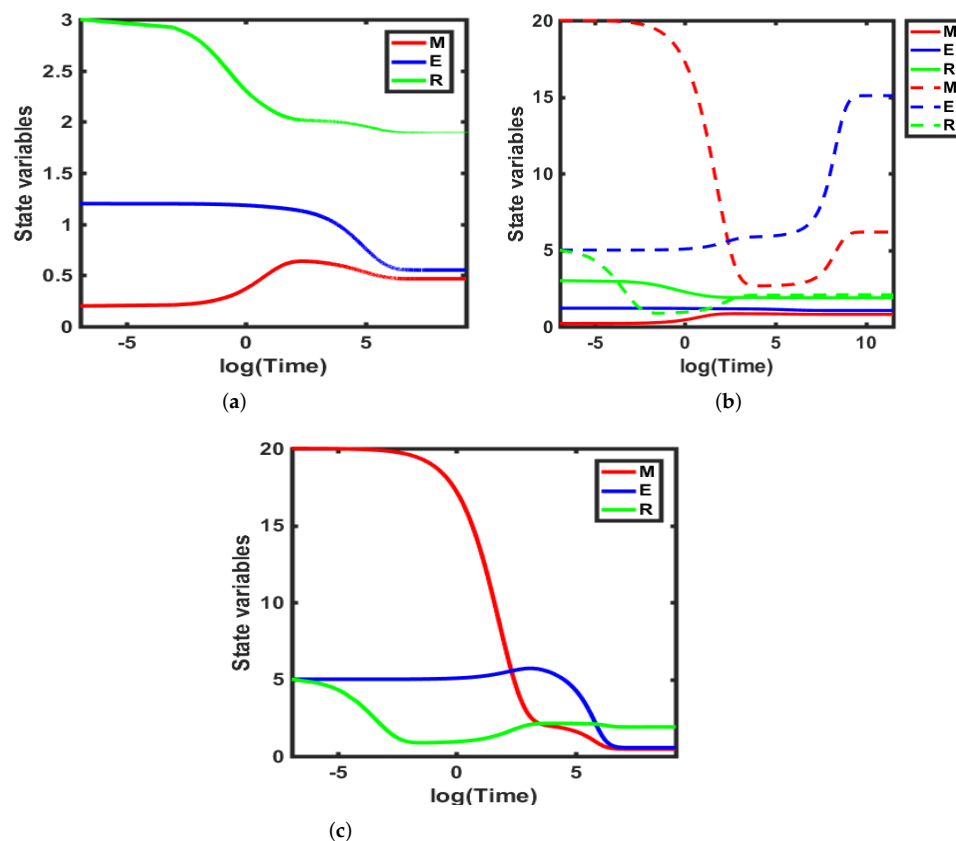


Figure 3. Numerical simulations illustrating the time evolution dynamics of $(M(t), R(t), E(t))$ for system (1) corresponding to different dynamic regimes. As the value of GF increases, the system transitions from stable ((a) with $GF = 0.3$ and initial conditions $M_0 = 0.2$, $E_0 = 1.2$, $R_0 = 3$) through bistable ((b) with $GF = 0.39$ and two sets of initial conditions $M_0 = 0.2$, $E_0 = 1.2$, $R_0 = 3$ and $M_0 = 20$, $E_0 = 5$ and $R_0 = 5$) then back to stable ((c) with $GF = 0.45$ and initial conditions $M_0 = 20$, $E_0 = 5$ and $R_0 = 5$).

Second, we solved the system with the growth factor concentration GF value of 0.39 and two sets of initial conditions $M_0 = 0.2$, $E_0 = 1.2$, $R_0 = 3$ and $M_0 = 20$, $E_0 = 5$, $R_0 = 5$ while keeping all the other parameters fixed. The results obtained show that the system exhibits bistability, as shown in Figure 3b. Third, we solved the model after adjusting the growth factor concentration GF to 0.45 and, keeping all other parameters unchanged and initial conditions $M_0 = 20$, $E_0 = 5$ and $R_0 = 5$, the model evolves to a higher steady state, as shown in Figure 3c. These results confirm the conditions set in Theorem 2.

Next, we explored conditions given in Lemma 3 and Theorem 2, as demonstrated in Figure 4. Figure 4 illustrates numerically the dynamics of model system (1) when both Lemma 3 and Theorem 2 are violated. When both conditions of Lemma 3 and Theorem 2 are not satisfied, then there exist two steady states, one stable and another unstable, and, henceforth, the possibility of two different dynamics: either bounded (stable) or unbounded (unstable) solutions. The unstable steady state acts as a switch, determining the initial conditions under which the system may exhibit bounded or unbounded behaviour.

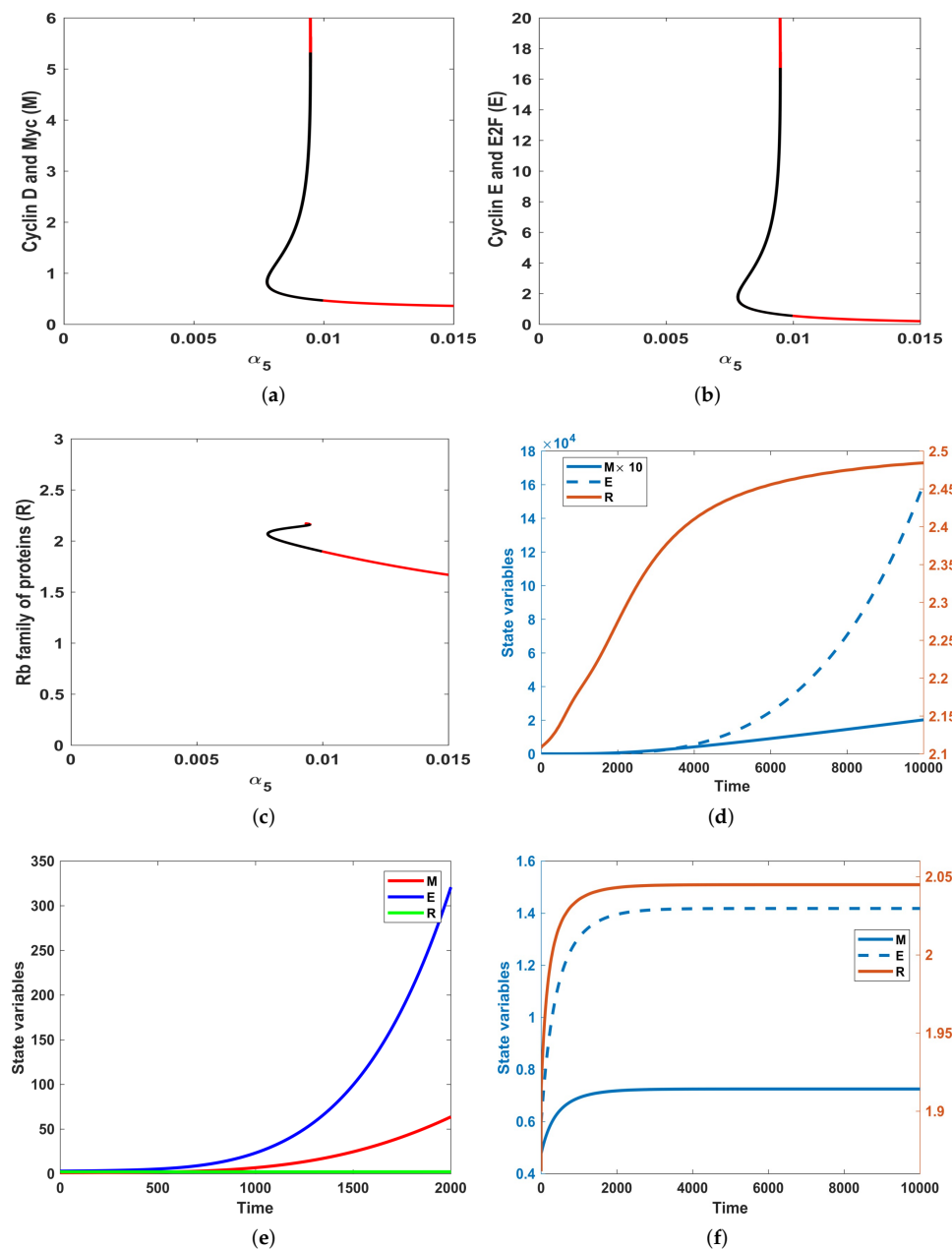


Figure 4. Numerical bifurcations and simulations illustrating the dynamics of System (1) where we explore the conditions of Theorem 2. (a–c) bifurcation diagrams for $M(t)$, $E(t)$ and $R(t)$, respectively, with respect to α_5 ; other parameter values are fixed as shown in Table 1 and $GF = 0.3$. (d) shows unbounded solutions of E and M with $\alpha_5 = 0.0079$, $\delta = 1$ and $GF = 0.3$, while keeping all the other parameters fixed as in Table 1 and initial conditions $M_0 = 1.2$, $E_0 = 3$, $R_0 = 1.2$ so that the conditions set in Theorem 2 and 3 are not met. To be more specific, $\gamma_2 > 0$, which is against conditions (A), (B) and (C) of Theorem 2. The $M(t)$ curve was amplified by a factor of 10 to visualize its behaviour with time and show that it grows unbounded with time while the R curve remain bounded because of conservation. (e) illustrates a zoom of the unstable dynamics of (d) for a short time $t \in [0, 2000]$ without scaling. (f) shows the stable time evolution of $M(t)$, $E(t)$ and $R(t)$ with $\alpha_5 = 0.0079$, $\delta = 1$ and $GF = 0.3$ with initial condition $(M_0, E_0, R_0) = (0.4782, 0.594, 1.8616)$. With these parameters, the model converges to the steady state $(M^*, E^*, R^*) = (0.7255, 1.4184, 2.0449)$.

To illustrate such dynamics, we set $\alpha_5 = 0.0079$, $\delta = 1$ and $GF = 0.3$, while keeping the rest of the parameters fixed, as shown in Table 1. This choice of parameters ensures that conditions (B) and (C) outlined in Theorem 2 are violated while, at the same time, the

$\min(\theta, \phi) = 0$, which violates Lemma 3. With this choice of parameters, model system (1) exhibits two steady states, as predicted above, an unstable and a stable steady state, which leads to either unbounded (unstable) or bounded (stable) solutions, respectively. Figure 4d demonstrates the validity of our theoretical results; the system of ODEs (1) becomes unstable with solutions for $M(t)$ and $E(t)$ growing unboundedly while those of $R(t)$ remain bounded. The biological justification for this type of model behaviour lies in our assumptions. Unlike the Rb family of proteins, which are assumed to be conserved for all time, $M(t)$ and $E(t)$ species are not conserved, because they are assumed to exist in abundance. Therefore, they are not constrained by laws of mass conservation. We also plot the bifurcation diagram as shown in Figure 4a, for which we have the lower stable steady state shown in red $((M^*, E^*, R^*) = (0.7255, 1.4184, 2.0449))$ with $\alpha_5 = 0.0079$, followed by an upper unstable steady state also for the same parameter value $\alpha_5 = 0.0079$ (shown in grey) $((M^*, E^*, R^*) = (0.9755, 2.25168, 2.08855))$. For completeness, we have included the bifurcation diagrams for $E(t)$ and $R(t)$, respectively, as illustrated in Figure 4b,c. The eigenvalues of the above steady states are given by $(-3.7119, -0.4209, -0.0015)$ and $(-5.6216, -0.3165, 0.0013)$, respectively, confirming that the lower steady state is stable while the upper is unstable. The unstable steady state acts as a switch mechanism between the unbounded and bounded solutions, determining the initial conditions under which the system may either exhibit unbounded or bounded solutions when conditions in Lemma 3 and Theorem 2 are violated.

We complete this section by illustrating stable dynamics of model system (1), as shown in Figure 4f. To obtain bounded solutions close to the unstable steady state, we adjusted our initial conditions to $M_0 = 0.4782$, $E_0 = 0.594$ and $R_0 = 1.8616$, such that these are located below the unstable steady state. The model system solved with this set of initial conditions exhibits bounded solutions which converge to the stable steady state computed above.

3.3. Sensitivity Analysis

Following the works in [56–58], we present the local sensitivity analysis of system (1) with respect to baseline parameter values in Table 1. We used local sensitivity analysis to identify the set of model parameters whose percentage change from the baseline parameter set causes significant changes in the model output [59]. Hence, local sensitivity analysis provides a useful insight into identifying model components that contribute most to the variability in the model output [59,60]. In general, there are two types of sensitivity analyses: local and global. In this article, we focused on local sensitivity analysis, which will allow us to evaluate changes in the model output with respect to variations in a single parameter at a time [59,61]. Global sensitivity analysis will allow for simultaneous changes in model parameters and evaluation of the interaction between parameters, which is not in our interest at this stage. Our methodology involves increasing parameters one at a time by 5%, and 10% and decreasing them by 5% and 10%, respectively. Next, we calculated the local sensitivity indices (percentage changes) in the solutions for $M(t)$, $E(t)$ and $R(t)$. The results for 5% increase, 5% decrease, 10% increase and 10% decrease are shown in Tables 2–5, respectively. We proceed to illustrate comparatively the results corresponding to 5% increase and decrease in Figure 5 as well as 10% increase and decrease in Figure 6 for each variable. First, we observe that the steady state M^* is mostly sensitive to parameters k_1 and GF , as shown in Figure 5a,b. Clearly, k_1 and GF have negative and positive effects to M^* , respectively, corresponding to 5% increase and decrease in parameters. This means that increasing k_1 reduces M^* , whereas increasing GF increases M^* . Second, the steady state E^* is mostly sensitive to α_2 and α_5 followed by k_1 , k_{r1} and GF , as shown in Figure 5c,d. Third, k_{r3} and α_2 have the greatest effect on R^* followed by α_4 and α_6 , as shown in Figure 5c,d. It is also pertinent to note that the effect of 5% parameter increases on the steady states of $M(t)$, $E(t)$ and $R(t)$ has a direct opposite effect to that of reducing the parameters by the same margin, as shown in Figure 5a–f. Furthermore, the response of $M(t)$, $E(t)$ and $R(t)$ steady-state values to a 5% increase in parameters is almost similar, as shown in Figure 5a,c.

In addition, the response of the $M(t)$, $E(t)$ and $R(t)$ steady-state values to a 5% decrease in parameters is also similar, as shown in Figure 5b,d, albeit with different magnitudes.

This can be interpreted biologically as follows: increasing (i) the growth factor concentration GF , (ii) the activation rate of $M(t)$, and (iii) the inhibition rate of $E(t)$ by $R(t)$ will result in an increase in the steady-state values of $M(t)$ and $E(t)$, leading to proliferation. Decreasing these parameters will reduce their respective steady states, leading cells to quiescence. In Figure 5e, all the parameters except α_2 , α_5 , β_2 , β_3 , k_{r1} , and k_{r2} have an opposite effect on the steady state of $R(t)$ when compared to those of $M(t)$ and $E(t)$, as shown in Figure 5a,c. Thus, increasing these parameters would have the effect of suppressing both M^* and E^* , as well as increasing R^* .

Table 2. Percentage changes in the steady-state values M^* , E^* and R^* after a 5% increase in parameter values of the non-linear model (1).

5% Increase in Parameter	% Change in M^*	% Change in E^*	% Change in R^*
k_1	−10.330	−10.186	0.7016
δ	−2.5797	−2.6158	−0.0973
α_6	−2.3573	−6.6279	1.7049
α_4	1.6213	4.5563	−1.1907
α_8	1.3212	3.7135	−0.96101
β_4	−1.4816	−4.1652	1.0916
k_{r3}	−3.6855	−10.361	2.78
α_5	3.6754	10.331	0.9486
β_2	0.9689	2.7222	0.1993
R_T	1.1586	3.2559	−0.8912
β_3	0.4682	1.3150	0.0671
k_{r1}	−2.1313	−5.9929	−0.73 16
α_2	−4.4144	−12.411	−1.5102
α_3	0.0008	0.00217	−0.0044
β_5	−0.50358	−1.4171	0.2834
k_{r2}	−1.3792	−3.8783	−0.5012
GF	8.2181	8.6153	−0.4477
β_1	4.8355	5.0458	−0.30391

Table 3. Percentage changes in the steady-state values M^* , E^* and R^* after a 5% decrease in parameter values of the non-linear model (1).

5% Decrease in Parameter	% Change in M^*	% Change in E^*	% Change in R^*
k_1	15.379	16.574	−0.74247
δ	3.0549	3.1573	−0.23624
α_6	2.7989	7.8667	−1.9380
α_4	−1.5130	−4.2539	1.0604
α_8	−1.3083	−3.6785	0.91636
β_4	1.4856	4.1750	−1.1118
k_{r3}	4.6941	13.194	−3.0811
α_5	−3.3974	−9.5522	−1.1635

Table 3. Cont.

5% Decrease in Parameter	% Change in M^*	% Change in E^*	% Change in R^*
β_2	−0.90100	−2.5340	−0.34861
R_T	−1.1643	−3.2747	0.77670
β_3	−0.47058	−1.3243	−0.22096
k_{r_1}	2.2750	6.3943	0.56813
α_2	5.6528	15.889	1.4395
α_3	−0.00076	−2.0707	0.00434
β_5	0.50506	1.4196	−0.37425
k_{r_2}	1.7225	4.8407	0.41722
GF	−7.5303	−7.4886	0.46275
β_1	−3.9715	−4.0111	0.25848

Table 4. Percentage changes in the steady-state values M^* , E^* and R^* after a 10% increase in parameter values of the non-linear model (1).

10% Increase in Parameter	% Change in M^*	% Change in E^*	% Change in R^*
k_1	−18.792	−18.005	1.5896
δ	−4.9970	−5.0238	0.25366
α_6	−4.5627	−12.828	3.5291
α_4	3.5450	9.9639	−2.4070
α_8	2.7918	7.8469	−1.9470
β_4	−3.1078	−8.7368	2.3944
k_{r_3}	−6.9382	−19.505	5.7536
α_5	8.0605	22.659	1.9911
β_2	2.1256	5.9736	0.52836
R_T	2.4269	6.8214	−1.7297
β_3	0.9800	2.7539	0.2105
k_{r_1}	−4.3112	−12.122	−1.4863
α_2	−8.2964	−23.324	−3.0332
α_3	0.0017	0.0047	−0.0093
β_5	−1.0545	−2.9658	0.7076
k_{r_2}	−2.6078	−7.3322	−0.8934
GF	18.296	19.8	−0.7814
β_1	11.815	12.677	−0.6242

Table 5. Percentage changes in steady-state values M^* , E^* and R^* after a 10% decrease in parameter values of the non-linear model (1).

10% Decrease in Parameter	% Change in M^*	% Change in E^*	% Change in R^*
k_1	43.284	51.402	−0.90841
δ	6.340764	6.6298	−0.40674
α_6	5.8216	16.364	−3.7086

Table 5. Cont.

10% Decrease in Parameter	% Change in M^*	% Change in E^*	% Change in R^*
α_4	−2.7912	−7.8475	2.0483
α_8	−2.4764	−6.9631	1.7939
β_4	2.8264	7.9439	−1.9852
k_{r_3}	10.236	28.774	−5.9032
α_5	−6.2295	−17.514	−2.2045
β_2	−1.6616	−4.6717	−0.56234
R_T	−2.2183	−6.2377	1.5914
β_3	−0.89676	−2.5224	−0.34685
k_{r_1}	4.44444	12.49	1.1354
α_2	12.394	34.839	2.8958
α_3	−0.0014110	−0.0038423	0.0081792
β_5	0.95936	2.6969	−0.73757
k_{r_2}	3.6812	10.3 47	0.94703
GF	−13.836	−13.470	1.0361
β_1	−7.0325	−7.0261	0.41178

Next, we proceed to investigate the correlations between parameter sensitivities to parameter changes for M against E , M against R and E against R , respectively, by considering a 5% increase in parameters. The results are shown in Figure 7. From Figure 7a, it is clear that all parameters except k_1 , δ , β_1 and GF affect the steady states M^* and E^* in the same way, since they lie on the same straight line. The parameters δ and k_1 have a negative effect on M^* , E^* and a positive effect on R^* , i.e., an opposite effect on R^* . Parameter GF has a positive effect on both M^* and E^* and an opposing effect on R^* . In Figure 7b,c, there is almost no correlation between the changes in the steady-state values M^* against R^* as well as E^* against R^* .

To proceed, we interpret the correlations shown in Figure 7. Generally, the order of the impact of parameters on $M(t)$ and $E(t)$ between a 5% and 10% increase in parameters is found to be similar, see Tables 2 and 4. This fact is also true for 5% and 10% decreases in parameters, as shown in Tables 3 and 5. This confirmed that none of the parameters of the system has a switching effect; that is, when they reach a particular threshold, their effect on the steady state is greatly increased, in relation to the other parameters. Having identified this, it is inferred that the dynamics of proliferation–quiescence transition remained unaltered with respect to small perturbations in parameters. In Figure 7a, most of the parameters are distributed linearly; thus, these parameters affect both $M(t)$ and $E(t)$ solutions in a similar fashion. Both Figure 7b,c show a similar pattern, in which parameter values are grouped in two well correlated sets. The first set contains parameters α_2 , k_{r_1} , k_{r_2} , β_3 , β_2 and α_5 , while the other contains k_{r_3} , α_6 , β_4 , α_3 , R_T , α_4 and α_8 . The effects of changes in α_3 are absolutely negligible, as shown in Figures 5 and 6. Biologically, α_3 represents the inhibition rate of R by E which is a two-stage process involving the dephosphorylation of the Rb family of proteins [40] followed by the inhibition of these proteins. This effectively means that the inhibition process depends on the dephosphorylation of the Rb family of proteins, thus explaining the negligible sensitivity observed in this case. The parameter δ lies off the linear pattern, as shown in Figure 7a, which is a result of its role in the proliferation–quiescence transition. It is known that variation in cyclin D levels through the cell cycle determines the proliferating fate of a cell [40]. Parameters δ , k_1 , α_1 and GF lie off the well-defined linear pattern followed by the rest of the parameters. From this

observation, it is inferred that a 10% increase in the inhibition rate of M (Cyclin D and Myc) causes a significant decrease in the activation of $E(t)$ (E2F, Cyclin E, Cyclin A) and a small increase in the activation of the Rb family of proteins. Under these circumstances, cells would naturally enter the quiescence state. Additionally, an increase in the expression of the Rb family of proteins significantly reduces the expression levels of E (E2F, Cyclin E and Cyclin A), thereby preventing cells from entering the cell cycle.

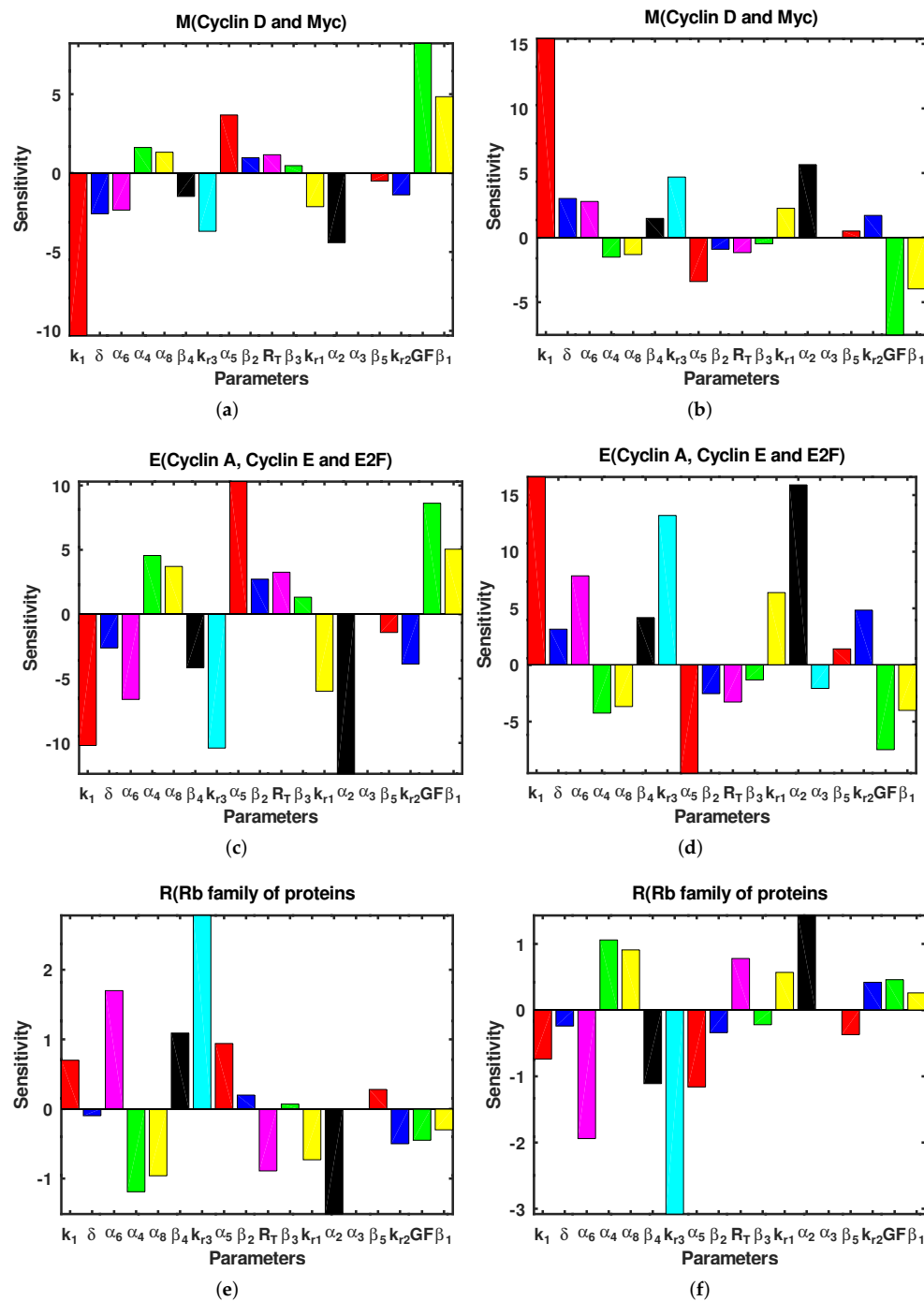


Figure 5. Parameter sensitivities for system (1) corresponding to 5% increase and decrease in parameters. (a,b) show sensitivity of M^* after 5 % increase and decrease in parameters, respectively; (c,d) show sensitivity of E^* corresponding to 5% increase and decrease, respectively. (e,f) show sensitivity R^* to 5% increase and decrease in parameters, respectively.

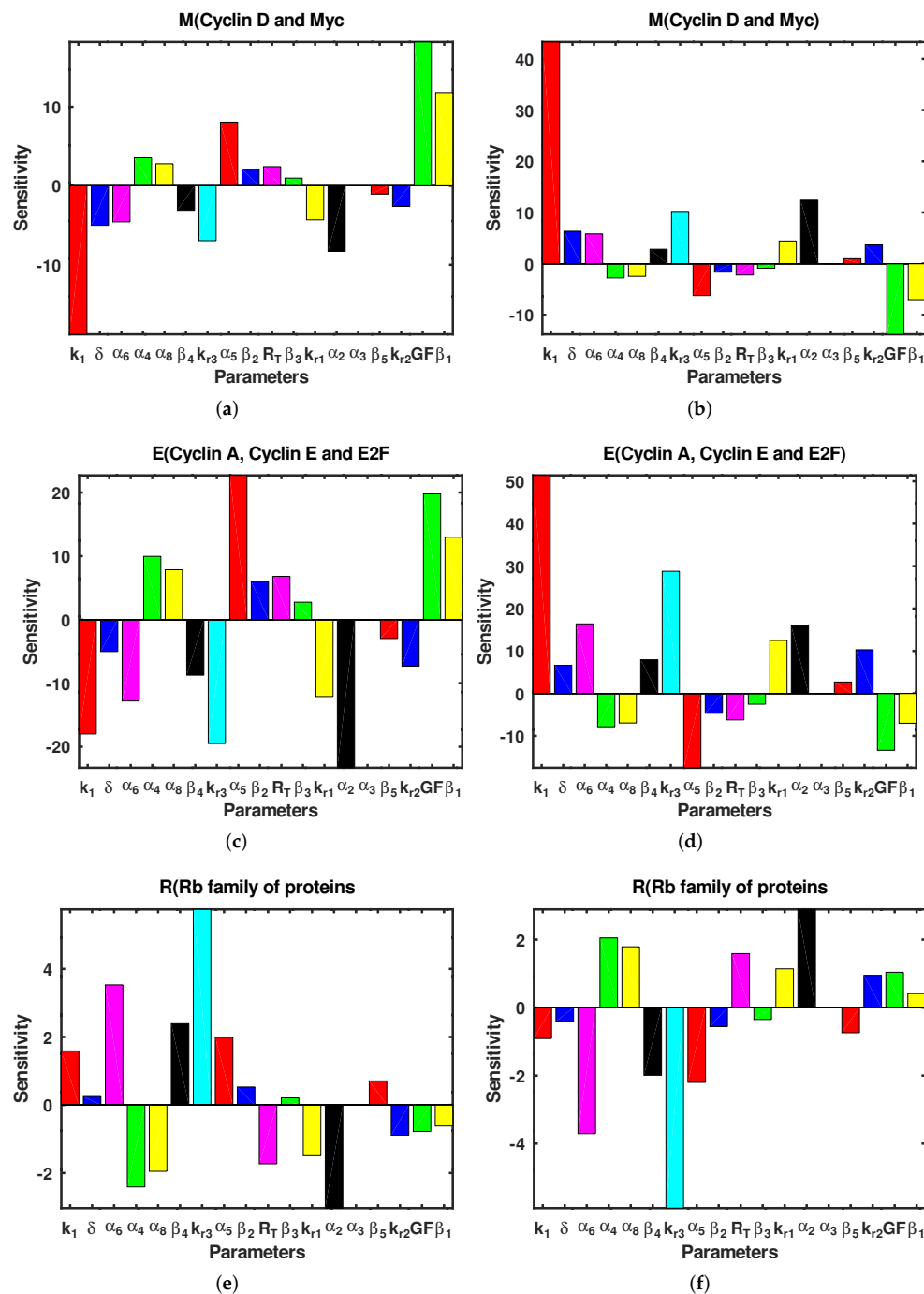


Figure 6. Parameter sensitivities for system (1) corresponding to 10% increases and decrease in parameters. (a,b) show sensitivity of M^* after 10 % increase and decrease in parameters, respectively, (c,d) show sensitivity of E^* corresponding to 10% increases and decrease, respectively. (e,f) show sensitivity R^* to 10% increases and decrease in parameters, respectively.

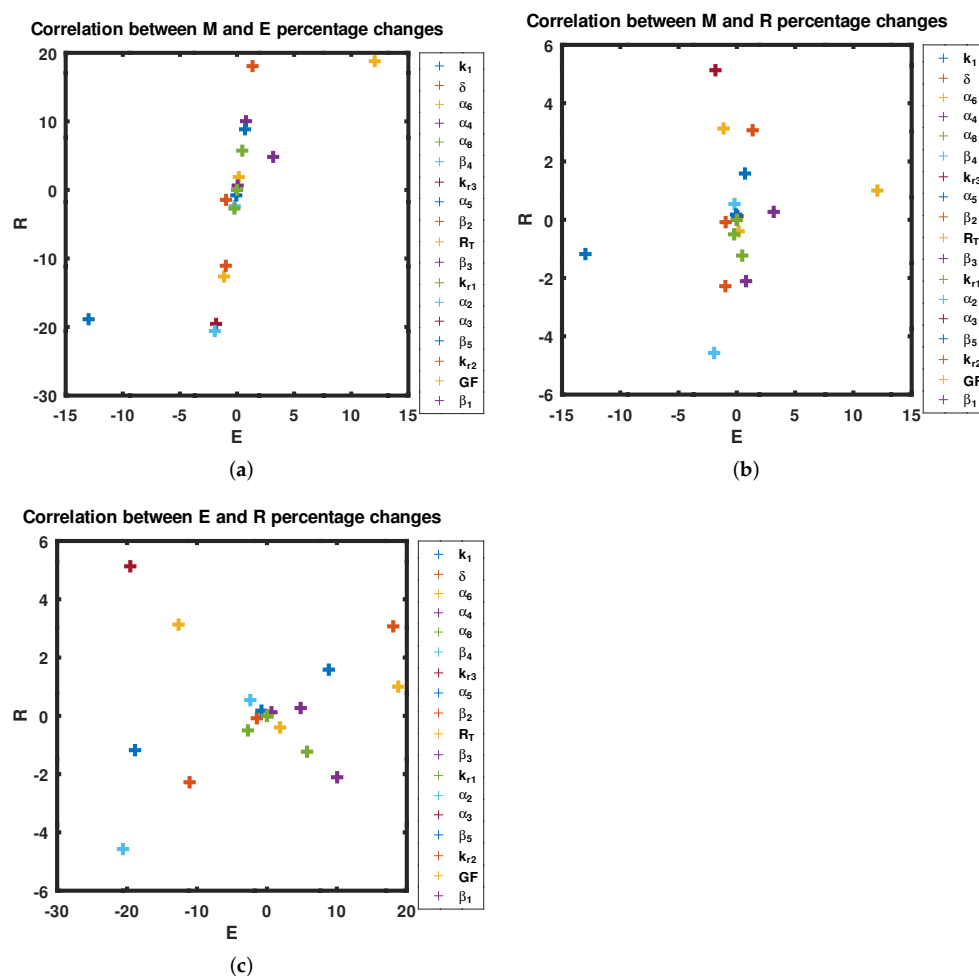


Figure 7. Correlation between parameter sensitivity of $M(t)$, $E(t)$ and $R(t)$ corresponding to 10% increase in model parameters. (a) shows the correlation between $M(t)$ and $E(t)$, (b) shows the correlation between $M(t)$ and $R(t)$ and (c) shows the correlation between $E(t)$ and $R(t)$.

4. Discussion

Biologically, it was shown that the growth factor concentration plays a pivotal role in a wide range of cellular processes, including cellular growth and differentiation [40]. As such, growth factor (GF) stimulation has a profound effect on cancer development [18,19,21]. Previous studies have shown that the $Rb - E2F$ bistable switch converts graded and transient serum growth signals into a binary and hysteric $E2F$ activity in individual cells [2].

In this paper

- Based on the concept of first principles, we investigated the dynamical potential of growth factors in the regulation of the cell-cycle entry.
- A mathematical model for the simplified $Rb - E2F$ network was constructed based on the model proposed in Yao et al. [2]. While previous studies modelled all links using Michaelis–Menten functions only [2], we used mass action, and Michaelis–Menten and Hill functions, resulting in a simpler model. In addition, we considered the R species to exist either in hyper-phosphorylated or hypo-phosphorylated form and that their total concentration is conserved.
- By varying the growth factor signal values through bifurcation analysis, numerical simulations illustrated that the magnitude of the value of the growth factor plays a critical role in regulating cell-cycle entry. Through bifurcation analysis, we deduced the existence of three consecutive dynamical behaviours, namely, stability, bi-stability and stability.

- Numerical simulations performed with different growth factor values validated the results derived from the bifurcation analysis. In particular, the biological interpretation of the uniform steady state can be established as follows:
 1. For $GF < 0.3735$, System (1) is asymptotically stable, indicating the regime in which cells are in a quiescent state. In this state, cells feature low levels of Cyclin D, Myc and high levels of R species.
 2. On the other hand, in the range $0.3735 < GF < 0.4138$, System (1) exhibits bi-stability, marking the position of the restriction point, as deduced in Yao et al. [42]. This point sets a high threshold separating quiescence from proliferation and acts as a barrier against unregulated and accidental cell growth. In addition, it provides a low-maintenance mechanism ensuring that the cell cycle proceeds, albeit later due to changes in the extracellular environment which is crucial for maintaining genome integrity.
 3. For values of $GF > 0.4138$, the system generates a stable dynamical behaviour where a cell is in the proliferation mode marking the higher steady state value. This state features high levels of Cyclin D, Myc and low levels of the Rb family of proteins.

However, it remains to investigate the conditions under which the system exhibits excitable and oscillatory dynamics as observed in a different model proposed in [62], but that would be investigated in a subsequent work. While Yao et al. [42] identified a basic gene circuit underlying resettable $Rb - E2F$ bi-stable switch controlling cell-cycle entry, we obtained a range of values of the growth factor concentration for the three dynamical regimes.

In this study, we focused our attention on the quantitative aspects of bi-stability, including ascertaining some constraints and the region for bi-stability, whereas, in [42], the focus was on the qualitative aspects of bi-stability.

Our consideration of the conservation of the R species did not affect the bistable nature of the system but revealed that the system becomes unstable at very low levels of the concentration of the R species. Local sensitivity analysis revealed that increasing parameters that enhance the availability of Cyclin A, Cyclin E, Cyclin D, Myc and E2F in the model results in the hyper-phosphorylation of Rb proteins. In its hyper-phosphorylated state, the Rb loses its affinity to bind free E2F, which results in transcription, leading to proliferation [40]. On the contrary, reducing these parameters by a small margin results in Rb dephosphorylation, which increases its affinity for E2F. Naturally, in its hypo-phosphorylated state, Rb binds to free E2F, impairing transcription. This results in cells being unable to pass through the restriction point and, hence, remaining in quiescence.

5. Limitations

In this study, we constructed an activator-inhibitor model to describe the $Rb - E2F$ signalling interaction network and analysed its dynamics and biological implications. However, in our study there are some limitations. Firstly, the model does not seem to exhibit periodicity and excitable dynamics. Secondly, spatial localisation of the proteins was completely ignored. This will give rise to partial differential equations. Thirdly, we did not fit the model to data to infer model parameters; this forms part of our future studies. Though simplification of the model produced the interesting bistable behaviour consistent with experimental observations, there were consequences on other dynamics of the $Rb - E2F$ signalling network such as oscillatory dynamics, as observed in [62]. Moreover, we assumed that all proteins other than the Rb family of proteins exist in abundance which may not be the case and hence must be investigated in future studies.

Author Contributions: K.Z.M. typed the manuscript, J.C.P. assisted in mathematical analysis as well as helped with editing the article. V.O.J. supervised the model formulation, numerical, bifurcation and sensitivity analyses as well as providing the Matlab codes. N.I.K. supervised most of the mathematical analysis as well as helped in editing the manuscript. A.M. conceived and supervised all aspects of the

study, including model formulation, analysis and simulations, as well as overseeing the manuscript write up. All authors have read and agreed to the published version of the manuscript.

Funding: All authors (K.Z.M., J.C.P., V.O.J., N.I.K., A.M.) acknowledge support from the EPSRC grant (EP/T00410X/1): UK–Africa Postgraduate Advanced Study Institute in Mathematical Sciences (UK-APASI) and from the African Diaspora Mathematicians Program—Developing international relations in Mathematics between the University of Zimbabwe (Zimbabwe) and Sussex (UK), Commission for Developing Countries (awarded to A. Madzvamuse and S. Mukwembi). A.M.’s work was partially funded by the Leverhulme Trust Research Project Grant (RPG-2014-149) and the European Union Horizon 2020 research and innovation programme under the Marie Skłodowska-Curie grant agreement (No 642866). This work (A.M.) was partly supported by Health Foundation (1902431), the NIHR (NIHR133761) and by an individual grant from the Dr Perry James (Jim) Browne Research Centre on Mathematics and its Applications (University of Sussex). A.M. is a Royal Society Wolfson Research Merit Award Holder funded generously by the Wolfson Foundation. A.M. is a Distinguished Visiting Scholar to the Department of Mathematics, University of Johannesburg, South Africa.

Data Availability Statement: The authors confirm that the data supporting the findings of this study are available within the article.

Acknowledgments: The authors wish to thank the University of Zimbabwe for funding the preliminary studies through the Graduate Teaching Assistantship Program (GTA). The authors also wish to thank G. Muchatibaya and colleagues in the University of Zimbabwe for supporting the research. AM thanks the International Mathematics Union, the Commission for Developing Countries and the UK Global Challenges Fund (through the Engineering and Physical Sciences Research Council) for supporting human infrastructure development and capacity building in Africa.

Conflicts of Interest: The authors declare that there is no conflict of interest regarding the publication of this paper.

References

- Wang, X.; Fujimaki, K.; Mitchell, G.C.; Kwon, J.S.; Croce, K.D.; Langsdorf, C.; Zhang, H.H.; Yao, G. Exit from quiescence displays a memory of cell growth and division. *Nat. Commun.* **2017**, *8*, 321. [[CrossRef](#)] [[PubMed](#)]
- Yao, G. Modelling mammalian cellular quiescence. *Interface Focus* **2014**, *4*, 20130074. [[CrossRef](#)] [[PubMed](#)]
- Harashima, H.; Dissmeyer, N.; Schnittger, A. Cell cycle control across the eukaryotic kingdom. *Trends Cell Biol.* **2013**, *23*, 345–356. [[CrossRef](#)] [[PubMed](#)]
- Miller, A.K.; Munger, K.; Adler, F.R. A mathematical model of cell cycle dysregulation due to human papilloma virus infection. *Bull. Math. Biol.* **2017**, *79*, 1564–1585. [[CrossRef](#)]
- Hartwell, L.H.; Weinert, T.A. Checkpoints: Controls that ensure the order of cell cycle events. *Science* **1989**, *246*, 629–634. [[CrossRef](#)]
- Kastan, M.B.; Bartek, J. Cell-cycle checkpoints and cancer. *Nature* **2004**, *432*, 316–323. [[CrossRef](#)]
- Naetar, N.; Soundarapian, V.; Litovchick, L.; Goguen, K.L.; Sablina, A.A.; Bowman-Colin, C.; Sicinski, P.; Hahn, W.C.; DeCaprio, J.A.; Livingstone, D.M. PP2A-mediated regulation of Ras signaling in G2 is essential for stable quiescence and normal G1 length. *Mol. Cell* **2014**, *54*, 932–945. [[CrossRef](#)]
- Nasmyth, K. Viewpoint: Putting the cell cycle in order. *Science* **1996**, *274*, 1643–1645. 1643. [[CrossRef](#)]
- Pardee, A.B. A restriction point for control of normal cell proliferation. *Proc. Natl. Acad. Sci. USA* **1974**, *71*, 1286–1290. [[CrossRef](#)]
- Qu, Z.; Weiss, J.N.; Maclellan, R. Regulation of mammalian cell cycle: A model of the G1-to-S transition. *J. Physiol. Cell Physiol.* **2003**, *284*, C349–C364. [[CrossRef](#)]
- Weinberg, R. The Biology of Cancer. In *Garland Science*; WW Norton & Company: New York, NY, USA, 2013; ISBN-13 978-0815342205.
- Zetterberg, A.; Larsson, O. Kinetic analysis of regulatory events in G1 leading to proliferation or quiescence of Swiss 3T3 cells. *Proc. Natl. Acad. Sci. USA* **1985**, *82*, 5365–5369. [[CrossRef](#)] [[PubMed](#)]
- Pandey, N.; Vinod, P.K. Mathematical modeling of reversible transition between quiescence and proliferation. *PLoS ONE* **2018**, *13*, e0198420. [[CrossRef](#)] [[PubMed](#)]
- Chen, H.Z.; Tsai, S.Y.; Leone, G. Emerging roles of E2Fs in cancer: An exit from cell cycle control. *Nat. Rev. Cancer* **2009**, *9*, 785–797. [[CrossRef](#)] [[PubMed](#)]
- Nevins, J.R. The Rb/E2F and cancer. *Hum. Mol. Genet.* **2001**, *10*, 699–703. [[CrossRef](#)]
- Nevins, J.R. E2F: A link between the Rb tumor suppressor protein and viral oncoproteins. *Science* **1992**, *258*, 424–429. [[CrossRef](#)]
- Yao, G.; Lee, T.J.; Mori, S.; Nevins, J.R.; You, L. A bistable Rb-E2F switch underlies the restriction point. *Nat. Cell Biol.* **2008**, *10*, 476–482. [[CrossRef](#)]
- Burns, F.J.; Tannock, I.F. On existence of a G0-phase in cell cycle. *Cell Tissue Kinet.* **1970**, *3*, 321.

19. De Maertelaer, V.; Galand, P. Some properties of a “G0” -model of the cell cycle. II. Natural constraints on the theoretical model in exponential growth conditions. *Cell Tissue Kinet.* **1975**, *8*, 11–22. [\[CrossRef\]](#)
20. Shields, R.; Smith, J.A. Cells regulate their proliferation through alterations in transition probability. *J. Cell. Physiol.* **1977**, *91*, 345–355. [\[CrossRef\]](#)
21. Smith, J.A.; Martin, L. Do cells cycle? *Proc. Natl Acad. Sci. USA* **1973**, *70*, 1263–1267. [\[CrossRef\]](#)
22. Castor, L.N. A G1 rate model accounts for cell cycle kinetics attributed to transition probability. *Nature* **1980**, *287*, 857–859. [\[CrossRef\]](#) [\[PubMed\]](#)
23. Koch, A.L. Does the variability of cell cycle result from one or many chance events? *Nature* **1980**, *286*, 80–82. [\[CrossRef\]](#) [\[PubMed\]](#)
24. Friend, S.H.; Bernards, R.; Rogelj, S.; Weinberg, R.A.; Rapaport, J.M.; Albert, D.M.; Drtja, T.P. A human DNA segment with properties of the gene that predisposes to retinoblastoma and osteosarcoma. *Nature* **2004**, *323*, 643–646. [\[CrossRef\]](#) [\[PubMed\]](#)
25. Tyson, J.J.; Chen, K.C.; Novak, B. Sniffers, buzzers, toggles and blinkers: Dynamics of regulatory and signaling pathways in the cell. *Curr. Opin. Cell. Biol.* **2003**, *15*, 221–231. [\[CrossRef\]](#)
26. Aguda, B.D.; Tang, Y. The kinetic origins of the restriction point in the mammalian cell cycle. *Cell Prolif.* **1999**, *32*, 321–335. [\[CrossRef\]](#) [\[PubMed\]](#)
27. Gardner, T.S.; Dolnik, M.; Collins, J.J. A theory for controlling cell cycle dynamics using a reversibility binding inhibitor. *Proc. Natl. Acad. Sci. USA* **1998**, *95*, 14190–14195. [\[CrossRef\]](#)
28. Goldbeter, A. A minimal cascade model for the mitotic oscillator involving cyclin and cdc kinase. *Proc. Natl. Acad. Sci. USA* **1991**, *88*, 9107–9111. [\[CrossRef\]](#)
29. Kohn, K.W. Functional capabilities of molecular network components controlling the mammalian G1/S cell cycle phase transition. *Oncogene* **1998**, *16*, 1065–1075. [\[CrossRef\]](#)
30. Norel, R.; Agur, Z. A model for the adjustment of the mitotic clock by cyclin and MPF levels. *Science* **1991**, *251*, 1076–1078. [\[CrossRef\]](#)
31. Nurse, P. The incredible life and times of biological cells. *Science* **2000**, *289*, 1711–1716. [\[CrossRef\]](#)
32. Obeyesekere, M.N.; Knudsen, E.S.; Wang, J.Y.J.; Zimmernan, S.O. A mathematical model of the regulation of the G1 phase of $Rb^{+/+}$ and $Rb^{-/-}$ mouse embryonic fibroblasts and an osteosarcoma cell line. *Cell Prolif.* **1997**, *30*, 171–194. [\[CrossRef\]](#) [\[PubMed\]](#)
33. Thron, C.D. Bistable biochemical switching and the control of the events of cell cycle. *Oncogene* **1997**, *15*, 317–325. [\[CrossRef\]](#) [\[PubMed\]](#)
34. Tyson, J.J.; Novak, B. Regulation of the eukaryotic cell: Molecular antagonism hysteresis, and irreversible transitions. *J. Theor. Biol.* **2001**, *210*, 249–263. [\[CrossRef\]](#)
35. Tyson, J.J.; Novak, B. Checkpoints in the cell cycle from modeler’s perspective. *Prog. Cell Cycle Res.* **1995**, *1*, 1–8. [\[CrossRef\]](#) [\[PubMed\]](#)
36. Novak, B.; Tyson, J.J. Modeling the control of DNA replication in fission yeast. *Proc. Natl. Acad. Sci. USA* **1997**, *94*, 9147–9152. [\[CrossRef\]](#)
37. Thron, C.D. A model for a bistable biochemical trigger of mitosis. *Biophys. Chem.* **1996**, *57*, 239–251. [\[CrossRef\]](#)
38. Aguda, B.D. A quantitative analysis of the kinetics of the G₂ DNA damage checkpoint system. *Proc. Natl. Acad. Sci. USA* **1999**, *96*, 11352–11357. [\[CrossRef\]](#) [\[PubMed\]](#)
39. Frolov, M.V.; Dyson, N.J. Molecular mechanisms of E2F-dependent activation and pRB-mediated repression. *J. Cell Sci.* **2004**, *117*, 2173–2181. [\[CrossRef\]](#)
40. Heldt, F.S.; Barr, A.R.; Cooper, S.; Bakal, C.; Novak, B. A comprehensive model for the proliferation-quiescence decision in response to endogenous DNA damage in human cells. *Proc. Natl. Acad. Sci. USA* **2017**, *115*, 2532–2537. [\[CrossRef\]](#)
41. Attwooll, C.; Denchi, E.L.; Helin, K. The E2F family: Specific functions and overlapping interests. *EMBO J.* **2004**, *23*, 4709–4716. [\[CrossRef\]](#)
42. Yao, G.; Tan, C.; West, N.; Nevins, J.T.; You, L. Origin of bistability underlying mammalian cell cycle entry. *Mol. Syst. Biol.* **2011**, *7*, 485. [\[CrossRef\]](#) [\[PubMed\]](#)
43. Blagosklonny, M.V.; Pardee, A.B. The restriction point of the cell cycle. *Cell Cycle* **2002**, *1*, 103–110. [\[CrossRef\]](#)
44. Gierer, A.; Meinhardt, H.A. A theory of biological pattern formation. *Kybernetik* **1972**, *12*, 30–39. [\[CrossRef\]](#) [\[PubMed\]](#)
45. Kamps, D.; Koch, J.; Juma, V.O.; Campillo-Funollet, E.; Graessl, M.; Banerjee, S.; Mazel, T.; Chen, X.; Wu, Y.; Portet, S.; et al. Optogenetic Tuning Reveals Rho Amplification-Dependent Dynamics of a Cell Contraction Signal Network. *Cell Rep.* **2020**, *33*, 108467. [\[CrossRef\]](#) [\[PubMed\]](#)
46. Sears, R.C.; Nevins, J.R. Signaling network that link cell proliferation and cell fate. *J. Biol. Chem.* **2002**, *277*, 11617–11620. [\[CrossRef\]](#) [\[PubMed\]](#)
47. Alon, U. *An Introduction to Systems Biology: Design Principles of Biological Circuits*; Chapman and Hall/CRC: New York, NY, USA, 2006; ISBN 9781439837177.
48. Michaelis, L.; Menten, M.L. Die Kinetik der Invertinwirkung. *Biochem. Z.* **1913**, *49*, 333–369.
49. Murray, J.D. *Mathematical Biology I: An Introduction of Interdisciplinary Applied Mathematics*; Springer: New York, NY, USA, 2002; pp. 257–271.
50. Henley, A.S.; Dick, F.A. The retinoblastoma family of proteins and their regulatory functions in the mammalian cell division cycle. *Cell Div.* **2012**, *7*, 1–14. [\[CrossRef\]](#)

51. Hsu, S.-B. *Ordinary Differential Equations with Applications*, 2nd ed.; National Hua University: Hsinchu, Taiwan, 2013; ISBN 978-981-4452-92-2.
52. Fine, B.; Rosenberger, G. *The Fundamental Theorem of Algebra*; Springer: New York, NY, USA, 1997.
53. Ermentrout, B. *Simulating, Analyzing, and Animating Dynamical Systems: A Guide to XPPAUT for Researchers and Students*; SIAM: Philadelphia, PA, USA, 2002; ISBN 978-0-89971-506-4.
54. Shampine, L.F.; Reichdt, M.W. MATLAB ODE Suite. *SIAM J. Sci. Comp.* **1997**, *18*, 1–22. [[CrossRef](#)]
55. Dormand, J.R.; Prince, P.J. A family of embedded Runge-Kutta formulae. *J. Comp. Appl. Math.* **1980**, *6*, 19–26. [[CrossRef](#)]
56. Juma, V.O. Data-Driven Mathematical Modeling and Simulations of Rho-Myosin Dynamics. Ph.D. Thesis, University of Sussex, Sussex, UK, 2019.
57. Juma, V.O.; Dehmelt, L.; Portet, S.; Madzvamuse, A. A mathematical analysis of an activator-inhibitor Rho GTPase model. *J. Comput. Dyn.* **2021**, *9*, 133. [[CrossRef](#)]
58. Zagkos, L.; Mc, Auley, M.; ; Roberts, J.; Kavallaris, N.I. Mathematical models of DNA methylation dynamics: Implications for health and ageing. *J. Theor. Biol.* **2019**, *462*, 184–193. [[CrossRef](#)] [[PubMed](#)]
59. Zhang, X.-J.; Trame, M.N.; Lesko, L.J.; Schmidt, S. Sobol sensitivity analysis: A tool to guide the development and evaluation of systems pharmacology models. *CPT Pharmacometrics Syst. Pharmacol.* **2015**, *4*, 69–79. [[CrossRef](#)] [[PubMed](#)]
60. Saltelli, A.; Chan, K.; Scott, E.M. *Sensitivity Analysis: Wiley Series in Probability and Statistics*; Jon Wiley: Chichester, UK, 2000; ISBN 978-0-470-74382-9.
61. Hampy, D.M. A review of techniques for parameter sensitivity analysis of environmental models. *Environ. Monit. Assess.* **1994**, *32*, 135–154. [[CrossRef](#)] [[PubMed](#)]
62. Yan, F.; Liu, H.; Hao, J.; Liu, Z. Dynamical behaviors of RB – E2F pathway including negative feedback loops involving miR449. *PLoS ONE* **2012**, *7*, e43908. [[CrossRef](#)]